

HIGH-VELOCITY SLURRY EROSION OF WELDED COBALT-BASED ALLOYS¹

Sebastian Romo²
Juan Felipe Santa²
Jorge Enrique Giraldo³
Alejandro Toro²

Abstract

Slurry erosion is an issue in components for pumping and power generation systems. Martensitic stainless steels have been widely used for such applications due to their corrosion resistance and moderate erosion resistance, although they must be regularly repaired by welding in order to extend their life. In this work, the slurry erosion resistance of a Co-based alloy used to repair and protect worn components by welding was tested in laboratory. The Co-based alloy was applied by manual welding onto 13Cr-4Ni steel and its slurry erosion resistance was compared to that of the substrate. The wear tests were done in a high-speed slurry erosion tester at an impact velocity of 25 ms⁻¹. The impingement angle varied between 15 and 90 degrees, the solids concentration of the slurry was 0.1 wt. % and the total duration of each test was 5 minutes. The microstructure of the coatings was studied by Optical and Scanning Electron Microscopy and, X-Ray Diffraction. The chemical composition was measured by Optical Emission, X-Ray Fluorescence and Energy-Dispersive Spectrometry. The slurry erosion resistance of welded Co-based alloys was higher than that of the substrate for all the studied impingement angles. The highest rationalized erosion rate was observed at an impingement angle of 45 degrees for both materials, being up to 50% lower for the Co-based weld overlays. In all cases, the worn surfaces showed ductile marks with micro-cutting as well as micro-ploughing. The microstructure of coatings was composed of M₇C₃ carbides in a Co-rich matrix, which suffered a phase transformation during wear process.

Keywords: Slurry erosion; Co-based alloy; Stainless steel.

EROSÃO DE ALTA VELOCIDADE EM LIGAS DE COBALTO APLICADAS POR SOLDAGEM

Resumo

A erosão é um problema em componentes para sistemas de bombeamento e geração de energia. Os aços inoxidáveis martensíticos têm sido amplamente utilizados para essas aplicações devido à sua boa resistência à corrosão e moderada resistência à erosão, embora os componentes devam ser regularmente reparados por soldagem a fim de prolongar a sua vida. Neste trabalho, a resistência à erosão de uma liga de Cobalto usada para reparar e proteger os componentes desgastados por soldagem foi testado em laboratório. A liga de cobalto foi aplicada por soldagem manual em aço 13Cr-4Ni e sua resistência à erosão em meio lamacento foi comparada com a do substrato. Os testes de desgaste foram realizados em uma máquina de erosão em meio lamacento com uma velocidade meia de impacto de 25 m·s⁻¹. O ângulo de impacto variou entre 15 e 90 graus, a concentração de sólidos da lama foi de 0.1% em peso e da duração total de cada teste foi de 5 minutos. A microestrutura dos depósitos de solda foi estudada por Microscopia Óptica e Eletrônica de Varredura e Difração de Raios X. A composição química foi determinada por espectrometria de emissão óptica, de energia dispersiva de Raios X (EDX) e de Fluorescência de Raios X (XRF). A resistência à erosão de ligas de Cobalto foi maior do que a do substrato para todos os ângulos estudados. A maior taxa de erosão racionalizada foi observada em um ângulo de incidência de 45 graus para ambos os materiais, sendo seu valor 50% menor para a liga de Cobalto. Em todos os casos, as superfícies desgastadas mostraram marcas dúcteis de micro corte e micro arado. A microestrutura dos revestimentos foi composta por carbonetos do tipo M₂₃C₆ numa matriz rica em Cobalto, a qual sofreu uma transformação de fase durante o processo de desgaste.

Palavras-Chave: Erosão em meio lamacento, Liga de Cobalto, Aço inoxidável.

¹ *Technical contribution to the First International Brazilian Conference on Tribology – TribobR-2010, November, 24th-26th, 2010, Rio de Janeiro, RJ, Brazil.*

² *Tribology and surfaces group, National University of Colombia, Medellín, Colombia*

³ *Welding Group, National University of Colombia, Medellín, Colombia*

1 INTRODUCTION

Martensitic stainless steels are used in important mechanical components of hydroelectric plants, such as turbines, injectors and valves. These materials have a good behavior under erosion and corrosion conditions, good weldability, high impact strength, high toughness, among other beneficial characteristics. Despite their good properties, martensitic steels experience surface damage due to the very demanding operating conditions in hydropower plants, which include cavitation and slurry erosion.⁽¹⁾

Wear is a major problem in hydroelectric power plants since it causes a reduction of operation efficiency and high costs due to downtimes, repairs, and replacement of the worn elements. Accordingly, the understanding of wear mechanisms is important to find solutions that contribute to enhance the components' life, and to lower replacement costs and maintenance. Build-up and protection of components in hydroelectric plants are usually carried out by electric arc welding due to the irregular form of some surfaces and the procedures are especially designed for each case due to particular susceptibility to cracking problems and presence of welding defects in the deposits.

The angle of impingement is important to determine the main wear mechanism acting on the surface of the components submitted to slurry erosion. It is well known that micro-cutting prevails for low impact angles whereas for angles close to 90° the dominant effects are low-cycle fatigue and accumulation of plastic deformation up to a critical value that promotes material's detaching.⁽²⁾

In this work, the wear resistance of a *Stellite 6* coating, which is widely recognized as a slurry erosion resistant material,⁽³⁾ was studied and it was compared with that of a martensitic stainless steel commonly used in components of hydroelectric power plants. High velocity slurry erosion tests were carried out varying the impingement angle to determine the maximum rationalized erosion rate of both materials.

2 EXPERIMENTAL PROCEDURE

2.1 Materials

The Shielded Metal Arc Welding (SMAW) process was used to apply *Stellite 6* coatings using Co-based surfacing electrodes onto ASTM A743 grade CA6NM martensitic stainless steel⁽⁴⁾(from now on, 13-4 steel); the welding parameters are presented in Table 1. *Stellite 6* specimens were welded in order to minimize dilution, i.e. to reduce alloying of the substrate with the coating material and no post-weld heat treatment was performed. The coatings were applied in two layers (Figure 1), and a grinding finishing procedure was carried out to remove 2 to 3 mm from the surface in order to obtain a flat surface. The 13-4 steel was received in the as-cast condition and it was homogenized at 1050 °C for 1 h and then air-cooled to room temperature. After that, the steel specimens were tempered at 620 °C for 1h and cooled down in air.

2.2 Microstructure and Chemical Characterization

The microstructure of *Stellite 6* coatings and 13-4 steel were analyzed in a Scanning Electron Microscope (SEM) and a Light Optical Microscope (LOM). The samples were ground with 240, 320, 400, 600, and 1000 emery papers and then taken to

polishing clothe with 3 μm diamond suspension. The characterization of the samples included Vickers hardness and micro-hardness measurements, X-Ray Diffraction (XRD) before and after the tests in a diffractometer operating with Cu-Kα radiation equipped with a 2D solid-state detector. The chemical composition was measured by Optical Emission Spectrometry (OES), Energy Dispersive X-Ray Spectrometry (EDXS) and X-Ray Fluorescence Spectrometry (XRFS).

Table 1. Welding parameters

| Welding Variable | Value |
|-----------------------------|---------|
| Process | SMAW |
| Preheat temperature (°C) | 150 |
| Inter-pass temperature (°C) | 150-200 |
| Welding current (A) | 90-120 |

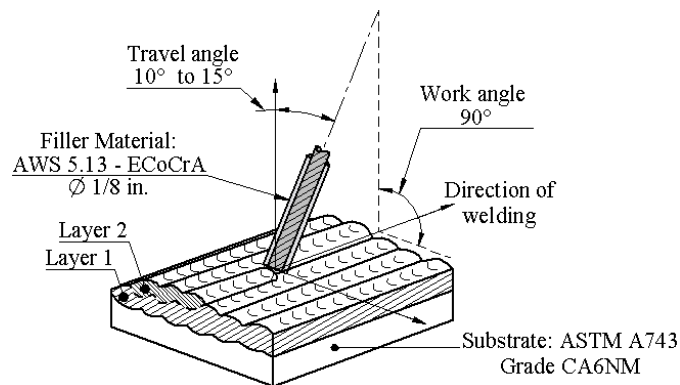


Figure 1. Schematic of the setup for deposition of *Stellite 6* by SMAW process.

2.3 Wear Tests

The slurry erosion tests were performed using a jet erosion testing machine shown in Figure 2. Slurry composed of tap water and SiO₂ particles impacted the surface of the samples at a velocity and angle of impact similar to those observed in some components of hydraulic turbines such as liners and runners. The typical aspect and sieve analysis of SiO₂ particles are presented in Figures 3a and b, respectively. The particles analyzed had an irregular sharp-edged morphology and the average Feret's diameter (FD), and Roundness Factor (F), were measured using digital image analysis. Circularity of the particles was calculated using equation [1] and its value for the abrasive particles used was $F = 0.4 \pm 0.2$, which indicates that the outline form of the particle, departs quite from circular.⁽⁵⁾ The Feret's diameter calculated was $FD = 0.6 \pm 0.1$ which is the longest distance between any two points along the sectional boundary of particle.

$$F = \frac{4rA}{p^2} \quad [1]$$

The parameters chosen for the slurry erosion tests are presented in Table 2. Only fresh slurry was used for each sample and the tests lasted 5 min with measurements of mass losses every minute. The worn surfaces were analyzed by LOM and SEM in order to identify the wear mechanisms and relate them to the mass loss results.

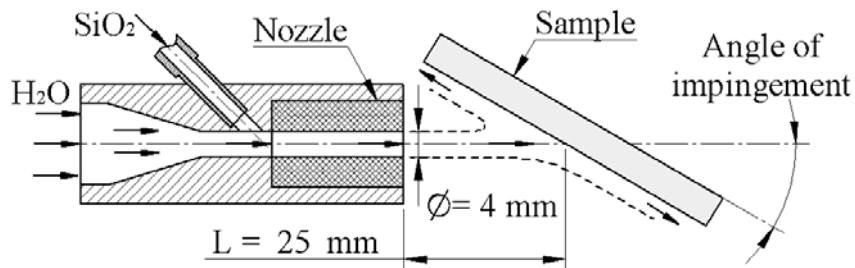
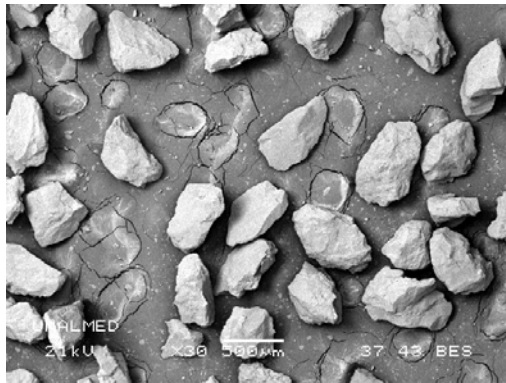
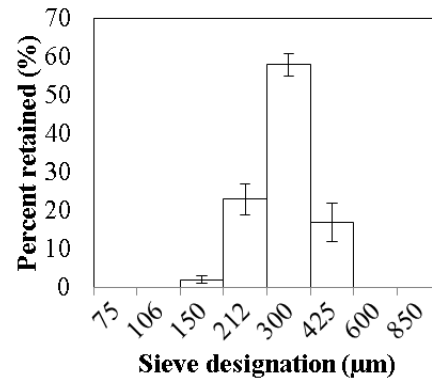


Figure 2. Schematic of jet erosion tests setup.



a)



b)

Figure 3. a) Typical morphology of the SiO₂ particles, b) Particle size distribution.

Table 2. Slurry erosion testing parameters

| Parameter | Value |
|--------------------------|---|
| Angle of impingement (°) | 15, 30, 45, 60, 75, 90 |
| Impingement speed (m/s) | 25 |
| Impinging medium | H ₂ O + SiO ₂ (0.1 wt. %) |
| Sand flow (g/min) | 18.8 |
| Erosion time (min) | 5 |
| Test temperature (°C) | 25 ± 1 |

3 RESULTS AND DISCUSSION

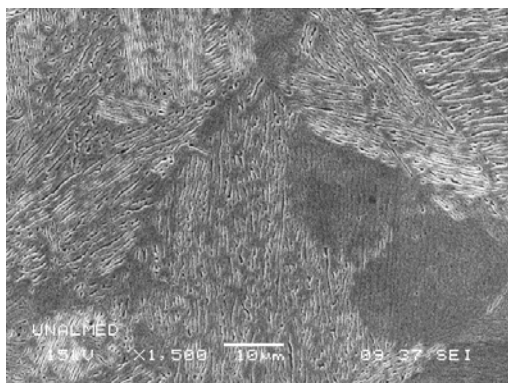
3.1 Characterization of *Stellite 6* and 13-4 Steel

The measured and nominal chemical compositions of *Stellite 6* coatings and 13-4 steel are presented in Table 3; it can be seen that the Fe content specified in AWS standard for the *Stellite 6* alloy, is higher in the obtained samples as a consequence of dilution during the welding process. Figure 4 shows the microstructure of both materials studied. The microstructure of 13-4 steel is composed of martensite, 15% retained austenite, and 4% delta ferrite, with an average hardness of 280 HV_{62.5}.⁽⁶⁾ *Stellite*'s microstructure is composed of a Co-rich, face-centered cubic α-phase and inter-dendritic carbides, with an average hardness on the second layer of 456 HV_{62.5}. Figure 5 shows the X-ray diffractograms obtained from *Stellite 6* samples where the peaks corresponding to matrix and carbides can be easily recognized.

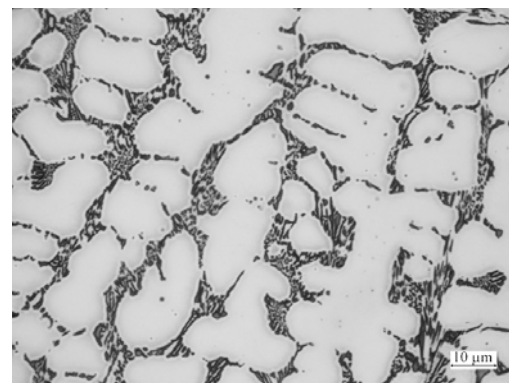
Additionally, a phase transformation after slurry erosion tests was observed. New diffraction peaks for epsilon-HCP martensite appeared near 42 and 72 degrees. Another important evidence of the existence of martensite is the increase in hardness values that will be discussed later in the section 3.2.1. On the other hand, the peaks corresponding with the M_7C_3 carbides did not appear after the slurry erosion tests. From worn surfaces it is possible to conclude that the carbides did not spall and according to that, the absence of that peak can be related to the final roughness of the surfaces causing a high noise on the X-ray pattern (note a small convex zone instead of a peak near its position). Further investigations must be done to conclude about this issue.

Table 3. Measured¹ and nominal² chemical composition of materials tested, Wt. %

| | Fe | C | Mn | Si | Cr | Ni | Mo | W | Co | Other Elements | |
|-------------------------------|-------|---------|-------|-------|-----------|---------|---------|---------|------|----------------|-------------------------|
| Stellite 6¹ | 12.84 | 0.86 | 0.301 | 1.42 | 27.8 | 2.56 | 0.114 | 3.54 | Bal. | Ti Va Ni | 0.119 0.071 0.049 |
| AWS 5.13² | 5.0 | 0.7-1.4 | 2.0 | 2.0 | 25-32 | 3.0 | 1.0 | 3.0-6.0 | Bal. | Total < 1.0 | |
| 13-4 steel¹ | Bal. | 0.052 | 0.693 | 0.802 | 12.733 | 3.769 | 0.509 | - | - | S P | 0.002 0.01 |
| ASTM A743² | Bal. | 0.06 | 1.00 | 1.00 | 11.5-14.0 | 3.5-4.5 | 0.4-1.0 | - | - | S P | < 0.03 < 0.04 |

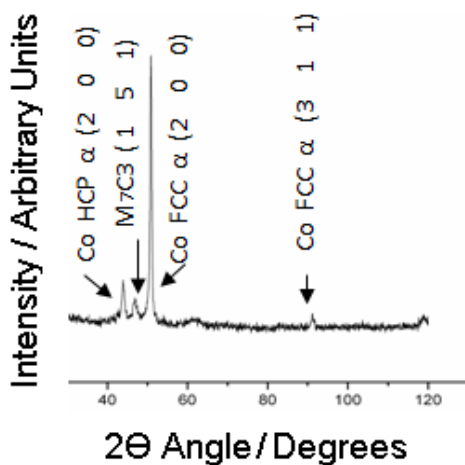


a)

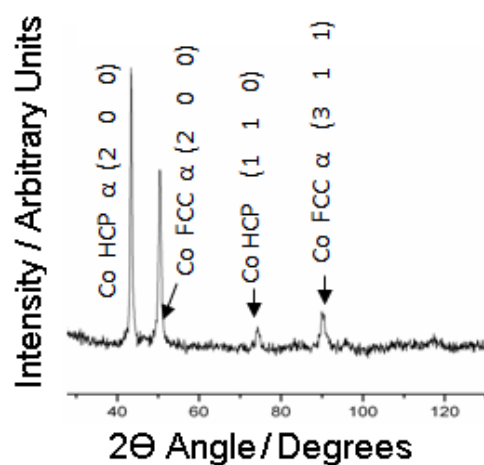


b)

Figure 4. Stainless steel and Co-based alloy microstructures, a) 13-4 Steel, SEM, b) Stellite 6, LOM.



a)



b)

Figure 5. XRD patterns of Stellite 6 coatings. a) Before testing b) After testing.

During the development of the welding procedure some transverse and crater cracks were observed as shown in Figures 6a and 6b. Those discontinuities correspond to problems associated with the weldability of this alloy. Transverse cracking has been related to differences in thermal expansion between the weld deposit and the base metal, which promotes residual stresses during cooling after welding.⁽⁷⁾ In this case, as a consequence of solidification behavior the coatings are susceptible to hot cracking. At the end of the solidification, compounds with low strength and melting point were formed at inter-dendritic spaces, causing cracking due to thermal contraction during cooling. Figure 6c shows evidences of the presence of Silicon, Titanium and Oxygen-rich compounds (according to EDX measurements) commonly used as de-oxidants in welding. Figure 6d shows the exposed dendrites once the low melting compounds were removed by etching.

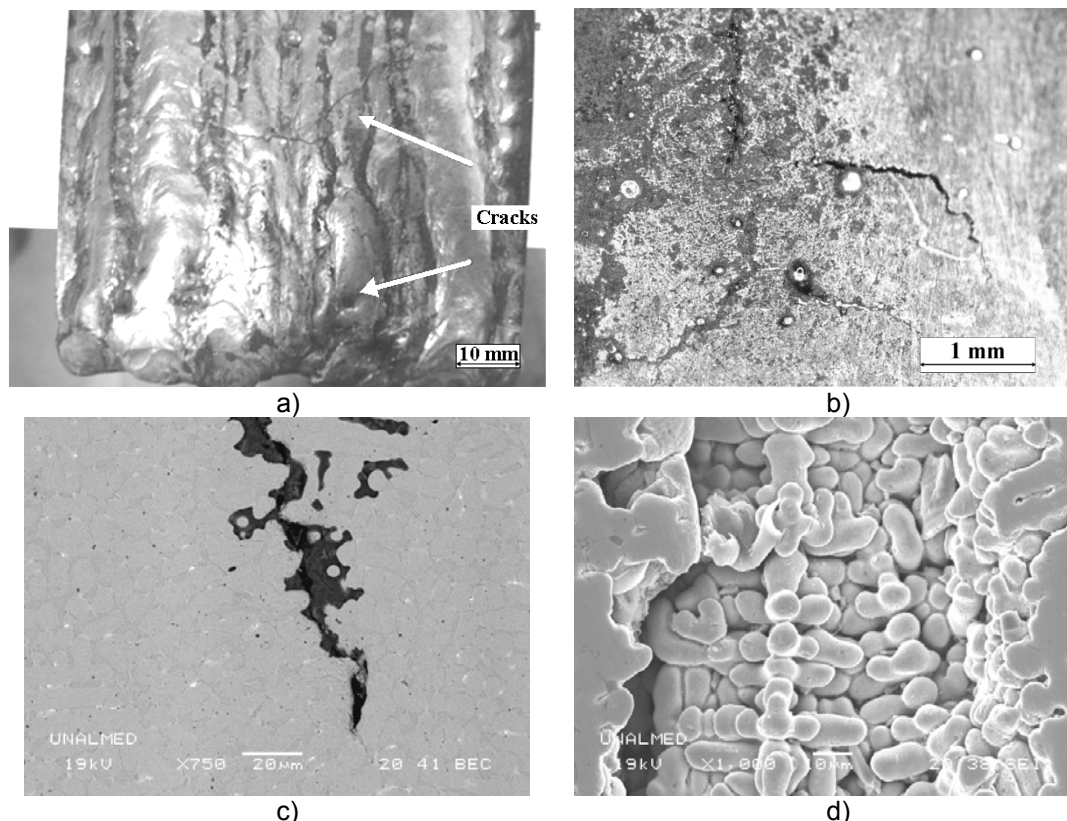


Figure 6. *Stellite 6* welding cracks. a) Crack at the end of the bead, LOM, b) Details of crater crack, LOM, c) **Backscattered** Electron Composition (BEC) image of low melting point compounds, and d) SEM micrograph of dendritic zones with removed low melting point compounds

3.2 Erosion Tests Results

Figure 7 shows the cumulative volume loss of the samples as a function of the testing time and Table 4 presents the variation in size of the eroded area of the samples as a function of the incident angle. The results showed that the highest slurry erosion resistance in *Stellite 6* was observed at an impingement angle of 15 degrees and the mass losses were higher at 30 and 45 degrees; the 13-4 steel showed a similar behavior with the impact angle. No running-in period (incubation period) was observed in any sample since the test is very severe and even after the first minute of exposure the coatings showed significant mass losses.

Since the cumulative mass loss curves are not appropriate to directly compare the erosion resistance of the materials for different impingement angles, a stricter criterion should be used to compare the results. The rationalized erosion rate R_e ,⁽⁸⁾ allows comparing the resistance of different materials and is calculated according to equation [2], where Q_e is the volumetric erosion rate ($m^3 \cdot s^{-1}$) defined as the slope of the cumulative volume loss curve shown in Figure 7; U_i is the impingement speed ($m \cdot s^{-1}$), and A the exposed area of specimen (m^2).

$$R_e = \frac{Q_e}{U_i A} \quad [2]$$

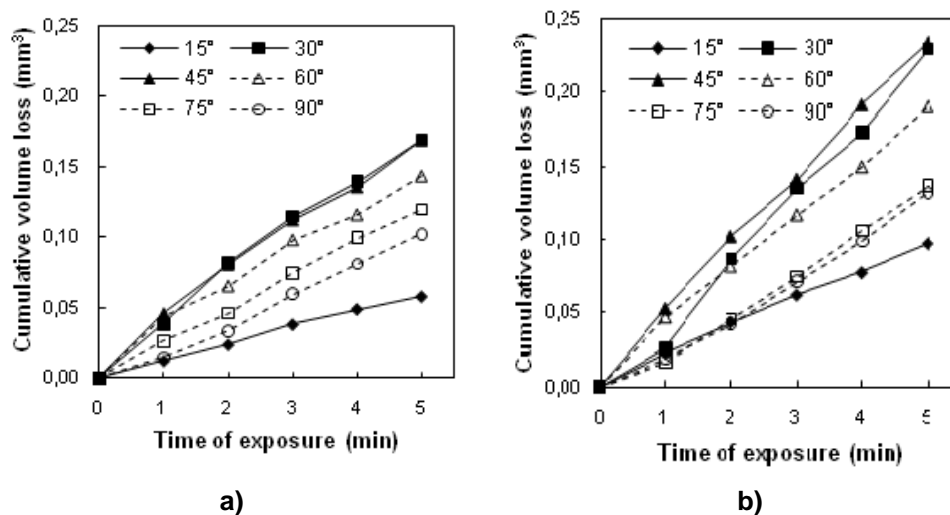


Figure 7. Cumulative mass losses of tested materials. a) Stellite 6, b) 13-4 Steel.

Table 4. Average area of wear marks (mm^2)



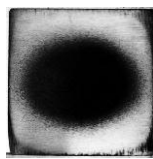
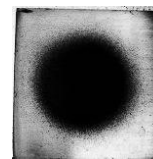
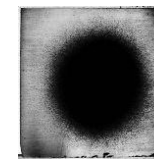
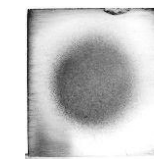

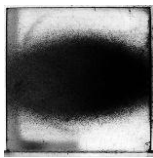
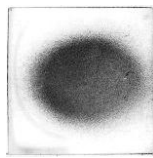
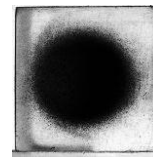
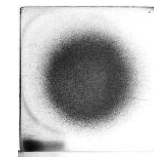
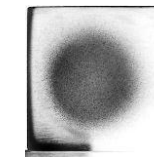
| | 15° | 30° | 45° | 60° | 75° | 90° |
|-------------------|---|---|---|--|---|---|
| Stellite 6 |  |  |  |  |  |  |
| | 154.3 | 172.7 | 152.1 | 152.8 | 153.7 | 134.1 |
| 13-4 steel |  |  |  |  |  |  |
| | 171 | 177.2 | 167.2 | 159.2 | 140.3 | 137.7 |

Figure 8 shows the rationalized erosion rate (RER) for the coatings and the substrate as a function of the impingement angle. It can be observed that the maximum erosion rate was found when the impingement angle was 45 degrees, which is a result

typically found in slurry erosion tests,^(9,10) as a consequence of the formation of a thin layer of fluid on the surface that helps protecting the material against the grazing impacts of solid particles. In dry erosion tests, this boundary layer does not exist and usually the maximum RER are observed at impact angles between 20 and 30 degrees. In both tested materials, RER showed a maximum at intermediate impingement angles (around 45 degrees), so it can be said that the ductile mode of erosive wear prevailed. The 13-4 steel can be considered a reasonably ductile material with a hardness of 280 HV, while the coatings are harder (456 HV) and more fragile. However, given the very strong dependence of the wear mechanisms on the speed of the erosive particle, with an impact velocity of 20 m/s it is possible for the material to behave in a ductile manner.

Figure 8 shows that the improvement in RER due to deposition of *Stellite 6* was higher for low impact angles, which means that hardness plays a key role on the slurry erosion resistance of the tested materials. A harder surface is more resistant to micro-cutting and micro-ploughing mechanisms, which are the dominating mechanisms under low impingement angle erosion.

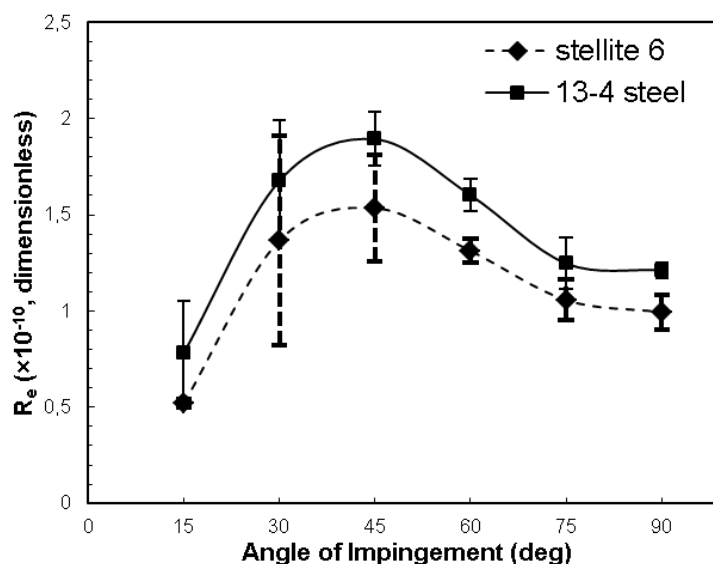


Figure 8. Rationalized erosion rate vs. Angle of impingement for tested materials.

3.2.1 Material removal mechanisms

Micrographs of eroded surfaces of *Stellite 6* and 13-4 steel are presented in Figures 9a to 9f for impingement angles of 15, 45, and 90 degrees. After low impingement angle tests, the worn surfaces show extensive plastic deformation and the main wear mechanisms observed are micro-cutting and micro-ploughing in both materials. For greater impact angles, on the other hand, the dominating wear mechanism was the detachment of highly deformed plates as a consequence of the repeated impact of particles over the surface although micro-ploughing and micro-cutting were still observed in a lesser extent. Drag forces due to the effect of the viscous medium (water in this case) can partially prevent the direct impact of particles against the surface, as stated by Stachowiak and Batchelor.⁽¹¹⁾ Also, as Bellman and Levi⁽¹²⁾ suggested, the removal of platelet-like edges created by impact extrusion may be responsible for significant mass losses under normal incidence conditions.

Generally speaking, the surface damage was more notorious in the samples tested with an impingement angle of 45 degrees. The length and depth of the grooves caused by the erodent particles were higher in this case, which is consistent with the

measured RER values. Additionally, hardness measurements performed in *Stellite 6* samples revealed an increase in this property as a consequence of the wear tests, passing from $647 \pm 17 \text{ HV}_{15 \text{ Kgf}}$ to $762 \pm 39 \text{ HV}_{15 \text{ Kgf}}$.

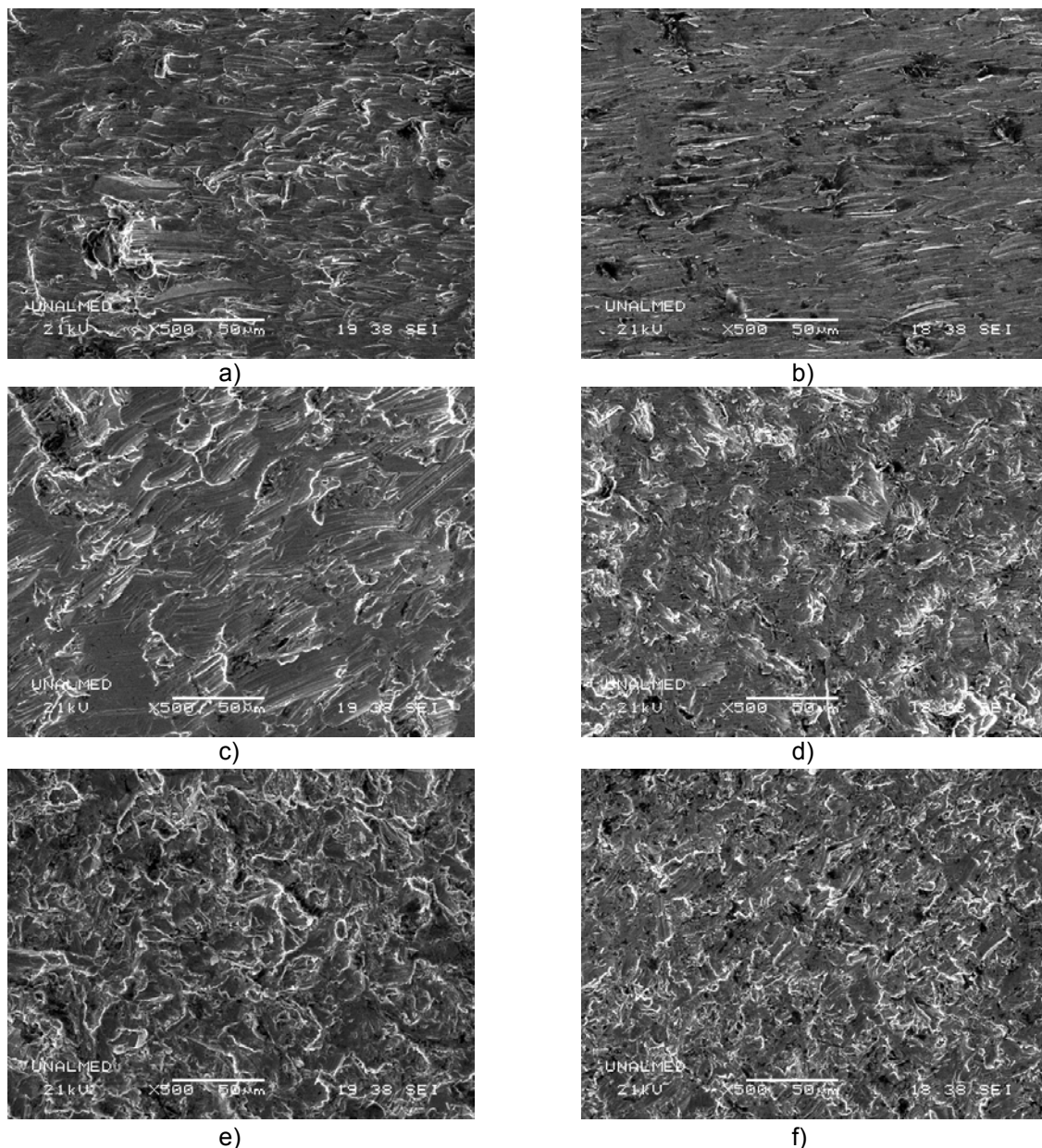


Figure 9. Aspect of the worn surfaces of tested material in slurry erosion. a) 13-4 steel. 15 degrees impact angle. SEM. 500 X, b) *Stellite 6*. 15 degrees impact angle. SEM. 500 X, c) 13-4 steel. 45 degrees impact angle. SEM. 500 X, d) *Stellite 6*. 45 degrees impact angle. SEM. 500 X, e) 13-4 steel. 90 degrees. SEM. 500 X, f) *Stellite 6*. 90 degrees. SEM. 500 X

4 CONCLUSIONS

- The microstructure of *Stellite 6* coatings is composed of dendrites of a FCC Cobalt-rich phase and Chromium complex carbides.
- The slurry erosion resistance of the *Stellite 6* coating was higher than that of 13-4 stainless steel for all the impact angles studied in terms of rationalized erosion rate (RER). The RER of the steel was 50% higher than the coatings for 15°, and between 18% and 23 % higher for 30°, 45°, 60°, 75° and 90° degrees.

- The dominant wear mechanisms acting on the surfaces were micro-cutting and micro-ploughing. In *Stellite 6* coatings, even when the impact angle was near 90° (and a brittle behavior would be expected), the response was mainly ductile; presumably as a result of drag forces acting on the surfaces.

Acknowledgements

The authors thank to *Dirección de Investigación* (DIME) of *Universidad Nacional de Colombia, Sede Medellín* for their financial support, DIME project No. 20201007791.

REFERENCES

- 1 *Study of cavitation in hydro-turbines - A review.* Kumar, Pardeep and Saini, R.P. 374-383, 2010, Renewable and sustainable energy reviews, Vol. 14.
- 2 **Zum Gahr, Karl Heinz.** *Microstructure and wear of materials.* Amsterdam : Elsevier, 1987. pp. 531-550. Tribology Series, 10.
- 3 **Crook, Paul and Levy, Alan V.** Friction and wear of Cobalt-base wrought alloys. *ASM Handbook: Friction, Lubrication, and Wear Technology.* 1992, Vol. 18, pp. 766-771.
- 4 **The American Society of Mechanical Engineers.** Specification for surfacing electrodes for shielded metal arc welding. *ASME Boiler & Vessel Code.* 2004, pp. 303-320. Section II, Part C.
- 5 **Hutchins, I. M. .** *Tribology: Friction and Wear of Engineering Materials.* London : s.n., 1992. págs. 135-140.
- 6 **Pacheco Gomez, Hernando.** *Transformaciones de fase causadas por un tratamiento termico posterior a la soldadura en acero inoxidable martensítico ASTM grado CA6NM.* Universidad Nacional de Colombia, Sede Medellín. Medellín : s.n., 2008. págs. 44-63.
- 7 **Williams, A.J., Rieppel, P.J. and Voldrich, C.B.** *Literature survey on weld metal cracking.* Ohio : s.n., 1952. pp. 46-48.
- 8 **ASTM International.** ASTM G73- 04: Standard Practice for Liquid Impingement Erosion Testing. 2004.
- 9 *Influence of microstructure on slurry erosive wear characteristics of laser surface alloyed 13Cr-4Ni steel.* Shivamurthy, R.C., et al., et al. 2009, Wear, Vol. 267, pp. 204-212.
- 10 *Slurry erosion studies on surface modified 13Cr-4Ni steels: Effect of angle of impingement and particle size.* Manisekaran, T, et al., et al. 5, 2007, Journal of materials engineering and performance, Vol. 16, pp. 567-572.
- 11 **Stachowiak, G.W. y Batchelor, A.W.** *Engineering Tribology.* Amsterdam : Elsevier, 1993. págs. 593-597. Tribology Series, 24.
- 12 *Erosion mechanism in ductile metals.* Bellman, Robert Jr y Levy, Alan. 1, 1981, Wear, Vol. 70, págs. 1-27.